January 2017

Novel Application Of Untargeted Metabolomics To Diseases Of Neurosurgical Significance

Alex Yang Lu
Yale University

Novel Application of Untargeted Metabolomics to Diseases of Neurosurgical Significance

A Thesis Submitted to the

Yale University School of Medicine

in Partial Fulfillment of the Requirements for the

Degree of Doctor of Medicine

by

Alex Yang Lu

2017

NOVEL APPLICATION OF UNTARGETED METABOLOMICS TO DISEASE OF NEUROSURGICAL SIGNIFICANCE.

Alex Y. Lu, Tore Eid, Veronica L. Chiang, Ketan R. Bulsara. Department of Neurosurgery, Yale School of Medicine, New Haven, CT.

Metabolomics, an emerging technique to study hundreds of small-molecule metabolites simultaneously, has been seldom applied to diseases of neurosurgical significance. We utilized metabolomics to explore two distinct questions: 1. to identify global metabolic changes and metabolite predictors of long-term outcome in aneurysmal subarachnoid hemorrhage (SAH) patients, 2. to identify differential metabolites profiles of radiation necrosis vs. recurrent tumor of metastatic brain lesions post-Gamma Knife radiosurgery. The first study applied gas chromatography time-of-flight mass spectrometry (GC-TOF) to cerebrospinal fluid samples collected from 15 high-grade aSAH patients (modified Fisher grades 3 and 4). Analysis was performed at two time points; metabolite levels at each time point were correlated with Glasgow Outcome Scale (GOS) of patients at 1 year post-aSAH. Of 97 metabolites identified, 16 metabolites (primarily free amino acids) significantly changed between the two time points; these changes were magnified in modified Fisher grade 4 compared with grade 3. Six metabolites (2-hydroxyglutarate, tryptophan, glycine, proline, isoleucine, and alanine) correlated with GOS at 1 year post-aSAH. These results suggest that specific metabolite changes occur in the brain during the course of aSAH and that quantification of specific CSF metabolites may be used to predict long-term outcomes. This is the first study to implicate 2-hydroxyglutarate, a known marker of tissue hypoxia, in aSAH pathogenesis. The second study applied GC-TOF to histologically-validated specimens (7 each) of pure radiation necrosis and pure recurrent tumor obtained from patient brain biopsies. Of 141 metabolites identified, 17 were found to be statistically significantly different between comparison groups. Of these metabolites, 6 were increased in tumor, and 11 metabolites were increased in radiation necrosis. An unsupervised hierarchical clustering analysis found that tumor had elevated levels of metabolites associated with energy metabolism whereas radiation necrosis had elevated levels of metabolites that were fatty acids and antioxidants/cofactors. This is the first tissue-based metabolomics study of radiation necrosis and tumor. Radiation necrosis and recurrent tumor following Gamma Knife radiosurgery for brain metastases have unique metabolite profiles that may be targeted in the future to develop non-invasive metabolic imaging techniques.

Acknowledgements

Deepest gratitude to Dr. Ketan Bulsara for his keen mentorship and for showing me the grace of a practicing neurosurgeon; to Dr. Veronica Chiang for her never-ending support and for showing me humor & humility in the practice of neurosurgery; to Dr. Tore Eid for introducing me to the exciting world of metabolomics.

This work was made possible with contributions from Eyiyemisi Damisah, Ryan Grant, Jack Turban, Lie Jie, Ahmed Alomari, and Alexander Vortmeyer.

Special thanks to the West Coast Metabolomics Center for their assistance with the methods section and to the Department of Neurosurgery, Yale School of Medicine for revealing to me my path to a fulfilling life--*to become more battlefield than man*.

Alex Lu received grant support from:

- James G. Hirsch MD Endowed Medical Student Research Fellowship,
- Marvin Moser Medical Student Research Fellowship
- Herman H. and Sarah Zusman Student Research Fellowships.

Disclosures

Portions of this work have been submitted for publication or previously published by the authors of this manuscript. These publications are:

- **Lu, A.Y.**, Damisah, E.C., Grant, R.A., Eid, T., Bulsara, K.R. Cerebrospinal Fluid Metabolomic Profiling of Aneurysmal Subarachnoid Hemorrhage Reveals Pathophysiology and Long-Term Outcome Predictors. Submitted.
- **Lu, A.Y.***, Turban, J.L.*, Damisah, E.K., Li J., Alomari, A.K., Eid, T., Vortmeyer, A.O., Chiang, V.L. Novel Biomarker Identification using Metabolomic Profiling to Differentiate Radiation Necrosis and Recurrent Tumor Following Gamma Knife Radiosurgery. *Journal of Neurosurgery.* In Press. DOI: 10.3171/2016.8.JNS161395

Table of Contents

Introduction

The Emergence of Metabolomics

During the last quarter century, the technology to investigate molecular mechanisms has rapidly evolved. Genomics and proteomics, the study of genome and set of proteins expressed by a genome respectively, have established themselves as leading fields of scientific inquiry. However, the study of genes and proteins without respect to downstream primary and secondary metabolites that they alter is limited. For example, when examining the most prevalent chronic diseases such as diabetes and cardiovascular pathology, the largest of genome-wide association studies only have described a modest fraction of these diseases and have provided partial insight mechanism-based intervention strategies[1-3].

Metabolites are defined as the small molecules such as amino acids, carbohydrates, nucleotides, and lipids that are transformed during an organism's metabolism. Metabolites can be grouped into several categories. When metabolites are produced by a host organism, they are considered to be endogenous metabolites whereas metabolites that originate from diet or the environment are considered exogenous metabolites. Most endogenous metabolites are also considered primary metabolites, biochemical compounds that are crucial for normal growth and development of an organism.

A biological sample's complete metabolite profile is defined as a metabolome. Metabolomics, the study of specific metabolomes, reveals a glimpse into the chemical fingerprint of an organism by identifying and quantitatively measuring hundreds to thousands of metabolites simultaneously. While humans possess an estimated 25,000

genes, 100,000 transcripts, and 1,000,000 proteins[3], human metabolome is estimated only to contain around 6,500 discrete small molecule metabolites[4]. While genes and proteins are modulated by epigenetic regulation and post-translational modifications respectively, metabolites represent the direct signatures of biochemical activity and therefore better correlate with an organism's state-specific phenotype[5]. This combination of these benefits makes metabolomics an ideal tool for clinical diagnostics as well as drug discovery.

Metabolomics can be divided into two general study types: targeted and untargeted. Targeted metabolomics is defined as the study of a specific number of predetermined metabolites. The work flow of targeted metabolomics originates with a hypothesis regarding the role or function of a predetermined metabolite within a predetermined biochemical pathway. With this approach, targeted metabolomics is particularly effective when applied to pharmacokinetic studies of drug metabolism and influence of genetic modifications or therapeutics on specific enzymes[6]. However, targeted metabolomics studies can only validate hypotheses and are limited when attempting elucidate novel molecular pathways. By comparison, untargeted metabolomics attempts to measure as many metabolites simultaneously as possible; however, this method provides limited control of what types of metabolites will be measured. Therefore, untargeted metabolomics provides global metabolite profiles, providing insight to biological processes that may have been previously uncharacterized. As a result, untargeted metabolomics is tool for hypothesis generation rather than hypothesis validation like that of targeted metabolomics.

The techniques to conduct metabolomics have rapidly evolved over the past decade. The workflow to generate and analyze metabolomics datasets are uniform: data acquisition, metabolite identification, and statistical analysis. Until the mid-2000s, nuclear magnetic resonance was the method of choice for the data acquisition and metabolite identification steps due to its highly accurate readings; however, nuclear magnetic resonance's limited metabolite sensitivity and specificity precluded global metabolite profiling. The current gold standard for metabolomics is mass spectrometry preceded by chromatographic separation (usually gas or liquid chromatography) to separate the highly complex mixture of metabolites in biological samples using the different chemical and physical properties of metabolites. Liquid chromatography uses a liquid mobile phase and is performed at room temperatures whereas gas chromatography utilizes a gas mobile phase and is performed at higher temperatures. Liquid chromatography has the advantage of being non-destructive to analyzed samples and can measure metabolites that are thermally labile. Gas chromatography can be performed faster, has higher resolutions, and provides higher peak resolution compared to liquid chromatography while also being less expensive to perform.

Mass spectrometry is advantageous compared to nuclear magnetic resonance due to its high sensitivity, reproducibility and versatility[7]. When a sample is processed, chromatographic separation yields a retention time for each unique metabolite. The masses of these metabolites and subsequent compound fragments are then measured by mass spectrometry, generating a mass-to-charge ratio. The combination of retention time and mass-to-charge ratio allows for the identification of thousands of metabolites simultaneously when compared to a standardized library of metabolite. In addition, mass

spectrometry generates relative intensities for each metabolite, allowing for quantification of metabolite levels. Many different mass spectrometry methods exist, each tailored for specific purposes. While triple quadrupole (QqQ) mass spectrometry is used for targeted metabolomics due to its high chemical sensitivity and specificity, quadrupole time-of-flight (Q-TOF) mass spectrometry is the method of choice for untargeted metabolomics studies.

Statistical analysis can be one of the most challenging aspects of conducting metabolomics. While targeted metabolomics can utilize workflows optimized to *a priori* knowledge of specific metabolites and metabolic pathways of interest, untargeted metabolomics generates complex data sets that require advanced computational tools to identify metabolite differences between samples and to examine each metabolite's relation to metabolic pathways and aberrant processes[7]. Some of these computational tools include multivariate statistical techniques (principal component analysis, partial least squares regression) and machine learning techniques (random forest, hierarchical clustering).

Because metabolomics techniques have existed for only the past two decades, several limitations exist. While many compounds can be detected using current technologies, many of the detected mass spectroscopy spectra have yet to be correlated to metabolites with known chemical structures. One study suggested that only 25% of observed compounds have been identified[8]. In addition, untargeted metabolomics can only provide relative quantification of metabolite levels and thus does not give measurement in SI units.

The applications of metabolomics have been diverse and is increasingly growing. Research areas that have utilized metabolomics have included plant biology[9], nutrition[10], and winemaking[11]. Within medicine, the bulk of metabolomics studies have focused on discovering and validating biomarkers within the fields of cancer[12], psychiatric disease[13], and microbiome[14]. The studies presented in this thesis utilize untargeted metabolomics due to its ability to identify novel metabolites/pathways and represent some of the first published studies to utilize untargeted metabolomics within issues of neurosurgical interest.

Subarachnoid Hemorrhage

Despite advancements in medical and surgical therapies, the clinical outcomes of aneurysmal subarachnoid hemorrhage (aSAH) have remained poor. Morbidity and mortality from subarachnoid hemorrhage and resulting complications are unacceptably high. Case fatality rate has been reported to be as high as 50%[15]; of those who survive, up to 40% of patients will suffer from long-term delayed neurological deficits such as stroke, hydrocephalus, and other ischemia-related disease[16]. These issues demonstrate the need for prognostic biomarkers that may better direct patient care. Although some potential biomarkers have been identified using human serum, cerebrospinal fluid, and urine, none are used clinically.

Cerebral vasospasm of large caliber vessels typically occurs between days 3 and 14 post-subarachnoid hemorrhage and has been thought to be a major contributor to morbidity and mortality; thus, cerebral vasospasm has been the historic target of intervention and biomarker identification studies. Around two-thirds of patients will

demonstrate some form (clinical vs. radiographic) of cerebral vasospasm during the post-subarachnoid hemorrhage period[17]. Current monitoring techniques includes frequent neurological examinations, transcranial Doppler ultrasonography, and computed tomography angiography (CTA) to examine changes in neurological status and vessel caliber. Therapies include oral or intra-arterial calcium channel blockers such as nimodipine, triple-H therapy (inducing hypertension, hypervolemia, and hemodilution), and balloon angioplasty. However, because cerebral vasospasm is a heterogeneous disease process combining pathology such as increased contraction of vascular smooth muscles cells, formation of microscopic thrombi in distal vessels, and inflammatory changes[18], no cerebral vasospasm biomarkers in serum or cerebrospinal fluid have been validated.

Recent clinical trials and literature have implicated other pathophysiologic factors as key contributors to poor patient outcomes of aneurysmal subarachnoid hemorrhage[19,20]. These factors include early brain injury, cerebral autoregulation disruption, electrolyte disturbances, oxidative stress, blood breakdown products, and inflammatory pathways[21]. Among these secondary sequaelae of subarachnoid hemorrhage, no clinical validated biomarkers exist[17]. Contributing to the lack of clinically useful biomarkers is the lack of knowledge regarding the pathophysiology of subarachnoid hemorrhage. Subarachnoid hemorrhage results in the vasculature of the brain, which is normally surrounded by cerebrospinal fluid (CSF), to be surrounded by a combination of blood, blood breakdown products, and cerebrospinal fluid. This altered cerebrospinal fluid and blood mixture triggers a cascade of unknown metabolic events

that disrupts all three layers of the blood vessels beginning around day 3 after the aneurysmal subarachnoid hemorrhage[22].

The high throughput profiling of metabolites, metabolomics, allows for the systematic analysis of the unique signature that cellular processes leave behind and can provide a chemical phenotype to the disease state. The identification of these signatures have been shown to have predictive and therapeutic value in other disease states[23,24]. For example, use of troponin level measurements has been proven to be one of the diagnostic tests with the highest sensitivity and specificity for acute myocardial infarction. Within the central nervous system, S100β and neuron-specific enolase as well as cerebrospinal fluid biomarkers creatinine kinase brain isoenzyme and neurofilament have been examined within the context of acute brain injury although the results of these studies have been mixed[25].

The aberrant metabolic processes of subarachnoid hemorrhage are currently unknown. In the first portion of this study, we report the results of applying untargeted metabolomics using gas chromatography with time-of-flight mass spectrometry (GC-TOF) to the cerebrospinal fluid of aneurysmal subarachnoid hemorrhage patients to determine global metabolic changes and metabolite predictors of long-term outcome in patient after aneurysmal subarachnoid hemorrhage.

Radiation Necrosis vs. Recurrent Tumor Conundrum

Gamma knife radiosurgery (GKRS) is a highly effective treatment for brain metastases especially when the tumors are multiple, small and surgically less accessible. The highly conformal delivery of radiation to the metastases results in relatively little

radiation exposure to the surrounding brain and preserves neurological status than the alterative, whole brain radiation. In a minority of cases, following an initial good response to GKRS treatment, the tumor being watched using magnetic resonance imaging (MRI) can start to regrow around 12 months after initial therapy. Radiographically, this appears as regrowth of the gadolinium-enhancing lesion on T1 weighted imaging associated with an increase in the amount of surrounding fluid-attenuated inversion recovery (FLAIR) signal. Histological examination of these re-growing lesions, however, can show either recurrent tumor or a treatment-related inflammatory process known as radiation necrosis. Radiation necrosis can be identified on histology by a central zone of coagulation necrosis surrounded inflammatory demyelination, astrocytosis, vascular hyalinization and reactive edema[26,27].

Despite clear histological differences and extensive research in the area, distinguishing radiation necrosis from recurrent tumor using non-invasive tests remains difficult. Currently available techniques for trying to differentiate the two entities include MR spectroscopy, MR perfusion, MR diffusion, and positron emission tomography (PET) imaging with tracers such as methionine-PET. While diagnostic accuracy rates of up to 80% have been reported at dedicated centers, the differentiation remains far from perfect when used in standard clinical practice. Differentiating the two processes, however, is vital to patient management decision making. Recurrent tumor may warrant further radiation treatment while radiation necrosis is typically managed with corticosteroids and other medical or surgical approaches since re-irradiation may worsen clinical status. To make the correct diagnosis, the current standard of care remains for these patients to undergo invasive brain biopsy or resection[28], exposing them to avoidable

surgical and perioperative risks that is also associated with considerable healthcare spending costs.

Given that radiation necrosis and tumor are distinct cellular processes, it would be expected that their metabolite profiles should also be distinguishable. The differences in their metabolite profiles could theoretically be used in conjunction with metabolite-based imaging to provide non-invasive differentiation of radiation necrosis vs. recurrent. In Metabolomic profiling using gas chromatography with time-of-flight mass spectrometry (GC-TOF) analysis allows investigators to evaluate a diverse range of low-molecular weight metabolites[29-31]. In this study, we implement GC-TOF on flash-frozen biopsy-confirmed radiation necrosis and tumor following GKRS to identify differential metabolite levels between the comparison groups and compare the identified metabolites to those currently used in metabolite-based imaging.

Statement of Purpose

First Study

- To identify global metabolic changes and metabolite predictors of long-term outcome in the cerebrospinal fluid of post-aneurysmal subarachnoid hemorrhage patients.

We hypothesize that CSF metabolomics profiles of aSAH patients change during the course of aSAH in an unknown manner and that these changes can be correlated to radiographic prognosticators such as the modified Rankin Score and to long term patient outcomes.

Second Study

- To identify differential metabolites profiles of radiation necrosis vs. recurrent tumor of metastatic brain lesions post-Gamma Knife radiosurgery

We hypothesize that the underlying distinctions in pathology between radiation necrosis and recurrent tumor of brain metastases lead to differential metabolite profiles; the identified metabolites within these profiles hypothetically would be useful in non-invasive diagnostic modalities such as imaging with magnetic resonance spectroscopy and positron emission tomography so that invasive testing such as brain biopsy and resection can be avoided.

Methods

Study Design (First Study)

We conducted a prospective observational study in 15 patients ≥ 18 years with aneurysmal subarachnoid hemorrhage, graded with modified Fisher score[32] and Hunt and Hess scale[33]. Aneurysms were clipped or coiled with external ventricular drains placed on day of admission or during surgical intervention according to instructional guidelines. Neurological examinations and transcranial Doppler sonography[34] were performed daily to assess for cerebral vasospasm[35], which was confirmed with CT angiography or formal catheter angiography. At the first year post-aSAH office visit, patients were evaluated using the Glasgow Outcome Scale (GOS)[36]. The study was approved by the Yale New Haven Hospital's Institutional Review Board. Informed consent for this study was obtained from either patients or their relatives at the time of cerebrospinal fluid procurement.

Daily CSF samples were collected from each patient while the ventriculostomy was in place. All patients had CSF samples collected on admission. This was compared to CSF from the first day that transcranial Doppler studies suggested at least moderate vasospasm. This was confirmed at a minimum with CT angiography. For those patients who had no radiographic vasospasm, CSF samples were selected on an average of post-bleed day 6.

Sample Preparation for GC-TOF (First Study)

After collection, CSF samples were immediately frozen and stored at -80°C until the time of simultaneous processing. For each sample, 5 µl of CSF were mixed with 1.0 mL of extraction solution (acetonitrile, isopropanol, and water in proportion 3:3:2). Samples were vortexed for 10 seconds and shaken for 5 minutes at 4°C using an Orbital Mixing Chilling/Heating Plate (Torrey Pines Scientific Instruments; Carlsbad, CA). Samples were then centrifuged for 2 minutes at 14000 rcf. The whole aliquot was evaporated using a Centrivap cold trap concentrator (Labconco, Kansas City, MO) to complete dryness and then re-suspended with 450 µl of degassed 50% acetonitrile. After being centrifuged for 2 minutes at 14000 rcf, the supernatant was removed, dried, and submitted for derivatization.

GC-TOF Methodology (First Study)

All samples were processed simultaneously and analyzed using GC-TOF according to published methodology in previously published studies[37]. An Agilent 6890 Gas Chromatograph (Agilent Technologies, Santa Clara, CA) with a Gerstel automatic

linear exchange and Gerstel cold injection system (Gerstel, Muehlheim, Germany) was programmed with the following temperature settings: 50°C to 275°C final temperature at a rate of 12 °C/s and hold for 3 minutes. The injection volume was 0.5 µl with an injection speed of 10 µl/s on a splitless injector with 25 seconds of purge time.

The gas chromatograph separation columns used in this study were of a 10 m long integrated guard column and a 30 m long, 0.25 mm Rtx-5Sil MS column (Restek, Bellefonte, PA) with a 0.25 µm 95% dimethyl/5% diphenyl polysiloxane film. The separations parameters consisted of 99.9999% ultra-pure helium with built-in purifier (Airgas, Radnor, PA) as the carrier gas at a constant flow rate of 1 mL/minute. Oven temperature was held at a constant 50°C for 1 minute and then increased by 20°C per minute up to 330°C, which was then held for 5 minutes.

The mass spectrometer used was a Leco Pegasus IV time-of-flight mass spectrometer with Leco ChromaTOF software (LECO Corporation, St. Joseph, MI). All samples were introduced at a transfer line temperature of 280°C. Electron impact ionization was set at 70 eV with a 250°C ion source temperature. For quality control, four calibrates and two blank samples were used in each run.

Data Processing (First Study)

Data processing followed previously published methodologies[37]. Using guidelines set by the Metabolomics Standards Initiative[38], GS/MS were annotated only if both retention index and mass spectra matched. The signals reported were then exported using the BinBase database, consisting of quantification ion, retention index, unique database identifier, and a complete mass spectrum string. The result files were transformed by

calculating the sum of all structurally identified compounds for each sample and by dividing all data with each sample by the corresponding metabolite sum; this value was then multiplied by a constant factor to obtain values without decimal places.

Data Analysis and Statistics (First Study):

All statistical analysis was performed using "R" version 3.2.3, a modular open-source programming suite (http://cran.r-project.org/). Data visualization was conducted with the "ggplot2" R-package. Metabolite levels at both time points were compared using principal component analysis and paired sample T-test with fold change threshold > 0.5. Metabolites levels at each time points were correlated with GOS using Pearson correlation. The significance threshold was $p<0.05$ with false discovery rate and Bonferroni corrections. The identified metabolite levels were compared with vasospasm development, modified Fisher grade, and Hunt and Hess scale by Mann Whitney *U* test or Pearson correlation. Metabolites that correlated with GOS were described with receiver operating characteristic curves to predict patients who had low disability (GOS=5) compared to moderate disability to death (GOS≤4).

Patient Cohort (Second Study)

All patients undergoing Gamma Knife radiosurgery at our institution sign consent for the details of their radiosurgery treatment and subsequent clinical course to be entered prospectively into a database. The names of patients who had to undergo surgical resection following radiosurgery were retrieved retrospectively and any available tissue

from these patients was retrieved from pathology achieves for this project according to institutional guidelines.

Collection and Pathologic Examination of Tissue Samples (Second Study)

All patients in this study had brain metastases that were treated with GKRS at the Yale Gamma Knife Center using the Leksell Gamma Knife 4C machine with radiosurgery dosing based on lesion volume as guided by RTOG-90-05 protcol[39]. At the time of lesional regrowth as seen by gadolinium-enhanced magnetic resonance imaging on follow-up imaging, each case was discussed at a multidisciplinary tumor board and each patient was selected to undergo surgical resection for optimal control of their regrowing lesions.

Immediately after surgical excision, all resected samples were bisected and processed in two different ways. Half of the sample was processed into formalin and paraffin for immediate surgical pathology diagnosis, while the other half was snap-frozen in optimal cutting temperature (OCT) compound. During retrospective identification of ideal radiation necrosis and recurrent tumor samples, sections of each sample from the paraffin block and frozen sections from the OCT block were concurrently examined histologically. Given that imaging changes after radiation can represent tumor regrowth, radiation injury or a combination of both, each specimen intended for metabolomics analysis was examined histologically first. Pure areas of radiation necrosis and pure areas of tumor were then separated from the resected specimens by neuropathologist Alexander Vortmeyer as shown in Figure 5. On histology, radiation necrosis was defined as three concentric rings of tissue with innermost necrosis, a middle region of reactive gliosis with

demyelination, and an outer ring of edema. As the distinguishing pathology, the middle region of reactive gliosis in the absence of tumor cells was separated from the other regions and sent for analysis after being matched to tumor sample of the same primary tumor type.

Upon dividing the surgical samples into either radiation necrosis or tumor, tissue samples were sectioned at -25°C to produce OCT-free 20-micron thick tissue flakes. Only areas of each histological slide with uniform histologic results (either radiation necrosis or recurrent tumor) were submitted for metabolomics analysis at the West Coast Metabolomics Center (Davis, California). The research study described here was performed with approval of Yale Pathology Tissue Services (YPTS Tissue Banking Protocol HIC# 304025173).

Sample Preparation for GC-TOF (Second Study)

For each sample, 4 mg of tissue was weighed and added to 1.0mL of acetonitrile, isopropanol, and water (3:3:2). The samples were homogenized using GenoGrinder and centrifuged at 2500 rpm for 5 minutes. The samples were then evaporated in a Labconco Centrivap cold trap concentrator and resuspended in 500 µl of 50% acetonitrile. After being centrifuged for 2 minutes at 14000 rcf, the supernatant was removed, evaporated, and submitted for two step derivatization with methoxyamine in pyridine followed by silylation with MSTFA (N-Methyl-N-(trimethylsilyl) trifluoroacetamide).

GC-TOF Methodology (Second Study)

The methodologies used were published in a previous study[37]. An Agilent 6890 Gas Chromatograph was equipped with a Gerstel automatic liner exchange system and a Gerstel cold injection system with temperature program as follows: 50°C to 275°C final temperature at a rate of 12 °C/s and hold for 3 minutes. Injection volume was 0.5 µl with 10 µl/s injection speed on a splitless injector with purge time of 25 seconds.

The gas chromatograph separation column consisted of a 30 m long, 0.25 mm Rtx-5Sil MS column with a 0.25 µm 95% dimethyl/5% diphenyl polysiloxane film and an additional 10 m integrated guard column. For the separation parameters, 99.9999% ultra pure helium with built-in purifier was used as a carrier gas at a constant flow of 1 mL/minute with oven temperature held constant at 50°C for 1 minute then increased by 20°C per minute to 330°C, which was held constant for 5 minutes.

A Leco Pegasus IV time-of-flight mass spectrometer controlled using Leco ChromaTOF software was used. The samples were introduced with a transfer line temperature set at 280°C. Electron impact ionization occurred at 70 eV with an ion source temperature of 250°C. Two blank samples and four calibrates were included in each run for quality control.

Data processing (Second Study)

GC/MS peaks were annotated only if identified according to Metabolomics Standards Intiative guidelines with both mass spectra and retention index recorded and matched. All signals were exported by the BinBase database, which was reported by quantification ion, a unique database identifier, retention index, and the complete mass spectrum encoded as string.

Result files were transformed by calculating the sum of all structurally identified compounds for each sample and by dividing all data associated with a sample by the corresponding metabolite sum. This value was multiplied by a constant factor to obtain values without decimal places; intensities of identified metabolites with more than one peak were summed to only one value in the transformed data set.

Statistical Analysis (Second Study)

Statistical testing was conducted using "R" version 3.2.3, a modular open-source programming suite (http://cran.r-project.org/). A principal component analysis was performed to check for discrimination accuracy between comparison groups using the "ropls" R-package. A random forest analysis utilizing the 10,000 trees was performed to obtain predictive accuracy metrics and a ranked list of metabolites based on importance to the classification scheme. The random forest analysis was conducted using the "randomForest" R-package.

Univariate statistical analysis included the Mann-Whitney *U* test and fold change between the comparison groups. Positive fold change values indicate elevated levels in radiation necrosis whereas negative fold change values indicate elevated levels in tumor. Statistical significance defined as $p < 0.05$ and fold change > 0.5. An unsupervised hierarchical clustering analysis was performed to obtain metabolomics subtypes within global metabolomics profiles to ascertain purported metabolic pathways, conducted using the "heatmap.plus" R-package. All data visualization was performed with the "ggplot2" R-package.

Author Contributions (Both Studies)

Alex Lu performed or was involved in the following:

- First Study: study design, all statistical analysis, all figure and table generation, manuscript drafting, and manuscript revisions.
- Second Study: study design, all statistical analysis, all figure and table generation, manuscript drafting, and manuscript revisions.

GC-TOF was performed by the West Coast Metabolomics Center (UC Davis, Davis, California) through their commercial metabolomics service.

Results

Patients and Descriptive Data (Study 1):

We enrolled fifteen patients with high-grade aneurysmal subarachnoid hemorrhage, defined by modified Fisher scale 3 or 4 (Table 1). The mean age was 55.73±16.98. Eleven (73%) patients were female. The mean Hunt and Hess score was 3.6±0.91. Nine patients (60%) developed vasospasm during their post-aSAH course. At one-year follow-up, 9 (60%) patients had no or low disability with Glasgow Outcome Score=5. Average post-bleed day collection at admission and during hospitalization were 1.06±0.7 and 5.53±2.0 respectively (Table 2).

Global Metabolite Changes:

GC-TOF identified 97 metabolites with known chemical structures. In a principal component analysis, the first and second principal components captured 19.4% and 14.5% respectively of the data variance (Figure 1). Sixteen metabolites (12 after

Bonferroni correction) changed significantly between the two time points (Table 3 and Figure 2A). In all these metabolites measured during hospitalization, the changes were magnified if patients had intraventricular hemorrhage and/or parenchymal extension (modified Fisher grade 4 vs 3), as shown in Table 3 and Figure 2B. Of the identified metabolites, no significant correlations were found after multiple correlation statistical correction with vasospasm development or Hunt and Hess scale.

One Year Outcome Predictors:

When correlating metabolite levels at each time point and GOS score, 6 metabolites measured during hospitalization correlated with GOS score (Table 4). 2-hydroxyglutarate was significant after Bonferonni correction (p=4.54e-4, Pearson=-0.79). Lower levels of all 6 metabolites correlated with better one-year outcomes post aneurysmal subarachnoid hemorrhage. When predicting patients who had no or low disability (GOS = 5), 2-hydroxyglutarate had a sensitivity of 0.89 and specificity of 0.83. The receiver operating characteristic curve of 2-hydroxyglutarate had an area-under-curve value of 0.85 (Figure 3A). The receiver operating characteristic curves for tryptophan, glycine, proline, isoleucine, and alanine had area-under-curve values of 0.67, 0.81, 0.80, 0.72, and 0.78 respectively.

At time of admission, 2-hydroxyglutarate levels in patients with GOS=5 and GOS≤4 were not statistically different (p=0.328) (Figure 3B). However, from time at admission to time during hospitalization, 2-hydroxyglutarate levels in patients with GOS=5 trended to decrease (p=0.22, fold change=-0.18) whereas 2-hydroxyglutarate levels in patients with GOS≤4 trended to increase (p=0.143, fold change=0.16), as shown

in Figure 4. In alpha-ketoglutarate, the precursor to 2-hydroxygluarate, alpha-ketoglutarate levels in patients with GOS=5 also trended to decrease (p=0.337, fold change=-0.087) whereas alpha-ketoglutarate levels in patients with GOS≤4 trended to increase (p=0.278, fold change=0.32), as shown in Figure 4.

Patient and Pathological Tissue Characteristics (Study 2)

Patient demographics and pathological specimen characteristics are summarized in Table 5 and Table 6. The average age of patients at the time of biopsy was 53.9 years. Two patients (20%) were male, and 8 were female (80%). Of the 10 patients, 4 contributed only radiation necrosis specimens, and 3 contributed only tumor specimens; 3 patients contributed both radiation necrosis and tumor specimens. As shown in Figure 5, tumor samples consisted of three primary tumor types: melanoma, breast, and non-small cell lung cancer (NSCLC). These tumor types represent the most common primary sites for central nervous system metastases.

Global Metabolite Analysis (Study 2)

Our protocol applied GC-TOF for pathologically confirmed radiation necrosis and recurrent tumor samples. In total, we identified 141 metabolites that could be confidently correlated to known biochemical structures. A principal component analysis of the global metabolite profiles suggests high discrimination accuracy between the comparison groups, shown in Figure 6A. The variance of the first and second principal component were 43.83% and 24.86% respectively.

A random forest analysis yielded an overall predictive accuracy of 78.57%. The random forest analysis also produced a ranked list of metabolites to distinguish the comparison groups. The top 25 metabolites are shown in Figure 6B.

Univariate Statistical Analysis of Identified Metabolites (Study 2)

Of the 25 metabolites identified with the random forest analysis, 17 metabolites had levels that were significantly different between radiation necrosis and tumor samples ($p < 0.05$ by Mann Whitney *U* test as shown in Table 7). These metabolites included alpha-tocopherol, proline, citric acid, gamma-tocopherol, UDP-glucuronic acid, butyrolactam, 2,5-dihydroxypyrazine, arachidonic acid, elaidic acid, taurine, UDP-N-acetylglucosamine, ribitol, adenosine-5-monophosphate, beta-sitosterol, conduritol-beta-expoisde, lauric acid, and putrescine. Of these metabolites, 6 metabolites were increased in tumor, and 11 metabolites were increased in radiation necrosis; all metabolites had an absolute fold change > 0.5 between comparison groups.

Metabolite Cluster Analysis (Study 2)

An unsupervised hierarchical clustering analysis of the identified 17 metabolites shows three distinct clusters of metabolites that discriminate the comparison groups of radiation necrosis vs. recurrent tumor (Figure 7). The three clusters represent increased metabolism (elevated in tumor), fatty acid products (elevated in radiation necrosis), and antioxidants/cofactors (elevated in radiation necrosis). The two metabolites that were most significantly elevated in radiation necrosis compared with recurrent tumor were alpha-tocopherol and citric acid. The two metabolites most elevated in recurrent tumor

compared with radiation necrosis were proline and UDP-glucuronic acid). Boxplots of the metabolite levels between comparison groups are shown in Figure 8. The receiver-operating curve of these metabolites have area-under-curve values of 1.00, 0.92, 0.94, and 0.93 respectively.

Analysis of Metabolites Currently Used in MR spectroscopy and PET (Study 2)

N-acetyl aspartate (NAA) along with creatine and choline are the metabolites currently used in MR spectroscopy for identification of radiation necrosis versus recurrent tumor. Of these 3 metabolites, only NAA was identified with this study's methodologies. NAA trended but was not found to be significantly elevated in radiation necrosis compared to tumor (p = 0.073, fold change 1.36). The boxplot and ROC curve of NAA with AUC value of 0.8.

In PET, analogs of glucose, are most commonly used although amino acids such methionine, phenylalanine and tyrosine have been studied at a few dedicated centers. Glucose and the individual amino acids were identified with this study's methodologies. The first quartile, median, and third quartile values of glucose trended to be higher in tumor compared to radiation necrosis but did not reach statistical significance (p = 0.53). Methionine, phenylalanine, and tyrosine also trended to be elevated in tumor compared radiation necrosis but again did not reach statistical significance (p = 0.62, 0.71, and 0.80, fold change = -0.17, -0.36, and -0.13 respectively). The receiver operating characteristic AUC values of glucose, methionine, phenylalanine, and tyrosine were 0.61, 0.59, 0.55, and 0.57 respectively.

Discussion

Study 1

Therapies that reduce cerebral vasospasm incidence have not produced better patient outcomes[19]. Successful biomarker identification in aneurysmal subarachnoid hemorrhage has been limited, and none are currently used in a clinical setting. In this exploratory study, we report the first use of untargeted metabolomics to screen large numbers of metabolites without the bias of theory-driven targeted metabolomics studies using cerebrospinal fluid in aneurysmal subarachnoid hemorrhage patients. This is also the first research study to implicate 2-hydroxyglutarate, a known biomarker of physiologic hypoxia in all human cells including neurons, in aneurysmal subarachnoid hemorrhage pathogenesis.

Our analysis identified metabolites (primarily free amino acids) that changed significantly during hospitalization; these changes were magnified if patients had intraventricular hemorrhage and/or parenchymal extension (modified Fisher grade 4 vs. grade 3). Similar changes in free amino acids have been identified in venous blood[40] of aneurysmal subarachnoid hemorrhage patients but were not associated with modified Fisher grade. While the cause of these metabolomics changes are unknown, two possible explanations are that these metabolites may be markers of increased blood breakdown and/or increased catabolism.

Our analysis also revealed a 6-metabolite panel that predicted long-term outcome independent of cerebral vasospasm development. Four of these metabolites (tryptophan, proline, isoleucine, alanine) significantly increased from time at admission to time during hospitalization. Glycine and proline are major components of collagen; induction of

meningeal collagen synthesis has been shown to be a pathologic hallmark of subarachnoid hemorrhage[41].

2-hydroxyglutarate can measured *in vivo* using MR spectroscopy[42] and is produced from alpha-ketoglutarate. 2-hydroxygluarate exists as two enantiomers: *L*-2-hydroxyglutarate and *D*-2-hydroxyglutarate. While *D*-2-hydroxyglutarate has been linked to glioma pathogenesis via mutant isocitrate dehydrogenase[43], *L*-2-hydroxyglutarate was recently implicated in all human cells as a universal physiologic adaptive response to hypoxia[44,45]. Human neuronal cells have been specifically shown to preferentially produce high levels of *L*-2-hydroxyglutarate in response to hypoxic stress[46]. High levels of *L*-2-hydroxyglutarate inhibit alpha-ketogluarate-dependent dioxygenases to regulate histone methylation levels and mitigate cellular reductive stress by inhibiting glycolysis and electron transport[44,45].

2-hydroxyglutarate has not been previously linked to stroke or stroke outcomes. We demonstrated that 2-hydroxyglutarate levels measured during hospitalization correlated with degree of recovery and could predict patients who had low disability at 1 year post-aSAH. While patients had similar levels of 2-hydroxyglutarate at admission, 2-hydroxyglutarate trended to increase in patients with moderate disability to death and trended to decrease in patients with low disability; these findings were mirrored in alpha-ketogluarate. Combined with previous literature, our results suggest that 2-hydroxyglutarate may be a marker of tissue hypoxia induced by global ischemia in aSAH.

This preliminary exploratory study has several limitations. The sample size and collection days of CSF were limited with only 15 patients with cerebrospinal fluid

metabolites levels measured at 2 time points reported. Future studies would benefit from cerebrospinal fluid measurements every day post-aSAH, allowing for increased resolution of metabolite levels post-aSAH. The addition of serum measurements of metabolite levels would also provide insight on global effects of aSAH and the relationship between serum and cerebrospinal fluid metabolite levels. Additional limitations include variability between cerebrospinal fluid collection days and no chiral discrimination of metabolites. Because this study design utilized untargeted metabolomics using GC-TOF, the data can only provide relative quantification so metabolites of interest would need to be measured using methods that provides SI units, which would be necessary to validate a clinically useful biomarker.

These results will need to be validated in a larger prospective study with increased temporal resolution and chiral analysis to differentiate the different enantiomers of 2-hydroxyglutarate. Knowledge about the specific metabolic changes in the brain during the course of aneurysmal subarachnoid hemorrhage may also provide important new insight into the pathophysiology of aneurysmal subarachnoid hemorrhage. In clinical practice, measurement of 2-hydroxyglutarate could be investigated as potential biomarker of ischemia after aneurysmal subarachnoid hemorrhage.

Overall, this is the first study to use untargeted metabolomics of CSF samples collected from aSAH patients for acute disease monitoring and long-term outcome assessments. The metabolites identified improve the current understanding of aSAH pathogenesis. 2-hydroxyglutarate may be used to predict patient outcomes and may represent a biomarker of global ischemia.

Study 2

A non-invasive method to differentiate radiation necrosis from recurrent tumor remains elusive but much needed today as the clinical use of radiosurgery increases[47] and patient survival continues to lengthen[48]. This study aimed to evaluate currently available imaging metabolites and validate their use specifically in differentiating radiation necrosis and metastatic tumor. In addition, this study aimed to identify novel metabolites that may serve as alternative *in vivo* biomarkers for imaging that would potentially outperform currently used metabolite imaging biomarkers.

In utilizing *in vivo* metabolite biomarkers, MR spectroscopy and PET would be the most promising imaging modalities. Current MR spectroscopy methods examine choline/creatine (Cho/Cr) and choline/N-acetyl aspartate (Cho/NAA) ratios. In this study, we were only able to measure NAA and therefore we were not able to make conclusions about the validity of using these ratios.

Current PET radiotracer analogs include glucose, methionine, phenylalanine, and tyrosine in the form of fluorodeoxyglucose (FDG), L-methyl-^{11}C-methionine (^{11}C-MET), 3,4-dihydroxy-6–^{18}F-fluoro-L-phenylalanine (^{18}F-FDOPA) and O-2-^{18}F-fluoroethyl-L-tyrosine (^{18}F–FET) respectively. For all these metabolites, the underlying assumption is that tumor is more metabolically active than radiation necrosis and accumulates higher levels of these metabolites. FDG-PET has been the most studied but suffers from wide ranges of reported sensitivities (65%-81%) and specificities (40%-94%)[49] depending on the institution and protocol used. Our results indicated that these 4 metabolites trended to be elevated in tumor compared to radiation necrosis, supporting the currently used PET methodology. However, the ability to discriminate between radiation necrosis and tumor

appear to be suboptimal compared to that of other candidate metabolites identified in our study.

We identified 17 novel metabolites that may have higher diagnostic potential if they can be translated into imaging studies. Our results suggest that radiation necrosis had elevated levels of fatty acids and antioxidant/cofactor metabolites whereas tumor had elevated energy metabolism markers.

In radiation necrosis, demyelination and cell death may result in increased fatty acid products; we identified lauric acid, ribitol, putrescine, putyrolactam, arachidonic acid, and elaidic acid as potential biomarkers within this group. Previous studies have found that oligodendrocytes are extremely sensitive to radiation[50,51]. In addition, MR spectroscopy of radiation necrosis often contains a large lipid peak, but no studies have resolved the involved metabolites[50,52,53]. The identified biomarkers in this study may contribute to this peak.

In addition, radiation necrosis tissue may mobilize elevated levels of antioxidants in response to oxidative stress and increased cell death within the local cellular niche. Our study identified the metabolites gamma-tocopherol, alpha-tocopherol, beta-sitosterol, citri acid, and conduritol-beta-epoxide as candidate biomarkers. While it is uncertain why these metabolites were elevated in radiation necrosis, one external explanation could be bias due to unreported patient oral supplementation. However, given that 3 patients contributed to both tumor and radiation necrosis samples, the likelihood of this bias is low.

Tumor is more anabolically active than normal tissue and likely more active than radiation necrosis; we found that tumor has increased levels of adenosine-5-

monophosphate, taurine, 2,5-dihydroxypyrazine, proline, UDP-glucronic acid, and UDP-N-acetyglucosamine. Taurine has been identified to be elevated in tissue samples of lung cancer tissue compared to paracancinomous tissue[54]. In addition, proline biosynthesis has been shown to augment tumor cell growth and aerobic glycolysis[55]. UDP-glucuronic acid and UDP-N-acetylglucosamine are both used by glucuronsyltransferase and glycosyltransferases reactions. Using UDP-N-acetylglucosamine as a substrate, multiple tumor types including breast, prostate, lung, liver colon, and bladder cancer have increased O-linked-β-N-acetylglucosamine modifications on intracellular proteins through the mTOR/MYC pathway[56]. Elevated levels of UDP-N-acetylglucosamine have also been found in human lung adenocarcinoma compared to nonmalignant tissue[57] as well as in human melanoma cells implanted in mice[58].

There are several limitations to this study. First, due to the low number of available tissue samples, no metabolites in the univariate statistical analysis reached significance with Bonferroni correction (significance threshold $p = 3.54e\text{-}4$). Although over 50 samples of resected tissue was examined, only 7 samples of radiation necrosis and 7 samples of recurrent tumor were pure enough in each pathology type to fit the criteria for study. This study was originally performed as a proof of concept study to determine if unique metabolites could be identified for radiation necrosis versus tumor. To the authors' knowledge, the study design of using flash frozen neural tissue post-resection in combination with metabolomics analysis has not been reported in the literature.

While several metabolites have been identified, the validity of our results still needs to be confirmed by further studies that include a larger sample size and a larger

variety of metastatic tumors. In addition, there are no data from this study to suggest that similar metabolites should be used to differentiate primary brain tumors from radiation necrosis. Second, this study does not provide any correlation with currently available imaging changes. While this would be the ultimate goal of solving the issue of differentiating radiation necrosis and recurrent tumor, the metabolites identified in the present would have to be translated into MR spectroscopy or PET imaging to become clinically useful. Third, this study does not address possible metabolite changes in pseudo-progression as it remains unclear if the pathophysiology of early post-radiation change such as pseudo-progression is the same as the delayed changes of radiation necrosis.

We acknowledge that these data are preliminary and that future work must be performed to validate these metabolites in combination with the development of in vivo neuroimaging modalities. If non-invasive imaging modalities can be developed specifically for the metabolites identified in this study, however, this may be the first step to robustly solving the current dilemma of distinguishing radiation necrosis and recurrent tumor after radiosurgery.

In summary, this study reports the first tissue-based untargeted metabolomics analysis of examining differential metabolic profiles of radiation necrosis versus tumor. The results identify multiple candidate metabolites that may be used with imaging modalities such as MR spectroscopy and PET imaging for differentiating radiation necrosis and tumor; these candidate metabolites may have much higher binary classification test results compared to those of currently used metabolites in MR spectroscopy and PET as suggested by tissue-based metabolomics results of the present

study. Although promising, a prospective study using the identified metabolites with radiographic techniques will be needed to test the applicability of these study results. If such study were successful, the need to ability to differentiate radiation necrosis and recurrent tumor using non-invasive imaging would eliminate the need for surgical resection in cases presenting without mass effect on local structures.

Conclusion:

These studies demonstrate the application of metabolomics to issues of neurosurgical importance. Future studies within neurosurgery may focus on the fields of traumatic brain injury, epilepsy, and brain cancer. Metabolomics is powerful tool to analyze the biochemical profile of any biological sample. The scale of high-throughput metabolomics is rapidly increasing. As metabolomics technology advances and workflows become optimized, the three areas of high-throughput metabolomics will increase cohort size, temporal resolution, and spatial resolution in future studies[17]. More patients will be included in these studies to allow for higher statistical power. The number of metabolites that can identified simultaneously will increase and the time it takes to analyze the high-throughput data will decrease. Finally, current metabolomics studies examine homogenized cell extracts or biofluids such as serum and cerebrospinal fluid. Future studies will be able to sample metabolome of single cells within subpopulation of interest.

The future of metabolomics will also rely on its integration with the ‘omics fields (genomics, transcriptomics, and proteomics) into a streamlined multi-omics platform. While the technology for combining these tools remains rudimentary, the multi-omics

approach has the potential to change the landscape of biomarker identification, drug discovery, and personalized medicine.

References

1. O'Rahilly S. Human genetics illuminates the paths to metabolic disease. Nature 2009.
2. Newgard CB, Attie AD. Getting biological about the genetics of diabetes. Nat Med 2010.
3. Newgard CB. Metabolomics and Metabolic Diseases: Where Do We Stand? Cell Metabolism 2016.
4. Wishart DS, Jewison T, Guo AC, Wilson M. HMDB 3.0—the human metabolome database in 2013. Nucleic acids … 2012.
5. Patti GJ, Yanes O, Siuzdak G. Innovation: Metabolomics: the apogee of the omics trilogy. Nature reviews Molecular cell biology 2012;13:263-9.
6. Nicholson JK, Connelly J, Lindon JC, Holmes E. Metabonomics: a platform for studying drug toxicity and gene function. Nature reviews Drug discovery 2002;1:153-61.
7. Johnson CH, Ivanisevic J, Siuzdak G. Metabolomics: beyond biomarkers and towards mechanisms. Nature Reviews Molecular Cell … 2016.
8. Baker M. Metabolomics: from small molecules to big ideas. Nature Methods 2011;8:117.
9. Schauer N, Fernie AR. Plant metabolomics: towards biological function and mechanism. Trends in plant science 2006.
10. Orešič M. Metabolomics, a novel tool for studies of nutrition, metabolism and lipid dysfunction. Nutrition 2009.
11. Schmidtke LM, Blackman JW, Clark AC. Wine metabolomics: objective measures of sensory properties of semillon from GC-MS profiles. Journal of agricultural … 2013.
12. Armitage EG, Barbas C. Metabolomics in cancer biomarker discovery: current trends and future perspectives. Journal of pharmaceutical and biomedical … 2014.
13. Xuan J, Pan G, Qiu Y, Yang L, Su M, Liu Y. Metabolomic profiling to identify potential serum biomarkers for schizophrenia and risperidone action. Journal of proteome … 2011.
14. Wikoff WR, Anfora AT, Liu J. Metabolomics analysis reveals large effects of gut microflora on mammalian blood metabolites. Proceedings of the … 2009.
15. Hop JW, Rinkel GJ, Algra A, van Gijn J. Case-fatality rates and functional outcome after subarachnoid hemorrhage: a systematic review. Stroke 1997;28:660-4.
16. Hong CM, Tosun C, Kurland DB, Gerzanich V. Biomarkers as outcome predictors in subarachnoid hemorrhage–a systematic review. Biomarkers 2014.
17. Zampieri M, Sekar K, Zamboni N, Sauer U. Frontiers of high-throughput metabolomics. Current Opinion in Chemical … 2017.
18. Przybycien-Szymanska MM, Ashley WW. Biomarker discovery in cerebral vasospasm after aneurysmal subarachnoid hemorrhage. Journal of Stroke and … 2015.
19. Macdonald LR, Higashida RT, Keller E, et al. Randomized trial of clazosentan in patients with aneurysmal subarachnoid hemorrhage undergoing endovascular coiling. Stroke 2012;43:1463-9.
20. Fujii M, Yan J, Rolland WB, Soejima Y, Caner B. Early brain injury, an evolving frontier in subarachnoid hemorrhage research. Translational Stroke Research 2013;4:432-46.

21. Cossu G, Messerer M, Oddo M. To look beyond vasospasm in aneurysmal subarachnoid haemorrhage. BioMed research … 2014.
22. Weir B, Grace M, Hansen J, Rothberg C. Time course of vasospasm in man. Journal of neurosurgery 1978.
23. Wang TJ, Larson MG, Vasan RS, Cheng S, Rhee EP. Metabolite profiles and the risk of developing diabetes. Nature medicine 2011.
24. Brindle JT, Antti H, Holmes E, Tranter G. Rapid and noninvasive diagnosis of the presence and severity of coronary heart disease using 1H-NMR-based metabonomics. Nature medicine 2002.
25. Chou SHY, Robertson CS. Monitoring biomarkers of cellular injury and death in acute brain injury. Neurocritical care 2014.
26. Alomari A, Rauch PJ, Orsaria M, Minja FJ, Chiang VL, Vortmeyer AO. Radiologic and histologic consequences of radiosurgery for brain tumors. J Neurooncol 2014;117:33-42.
27. Rauch PJ, Park HS, Knisely JP, Chiang VL, Vortmeyer AO. Delayed radiation-induced vasculitic leukoencephalopathy. Int J Radiat Oncol Biol Phys 2012;83:369-75.
28. Nath SK, Sheridan AD, Rauch PJ, et al. Significance of histology in determining management of lesions regrowing after radiosurgery. J Neurooncol 2014;117:303-10.
29. Kind T, Tolstikov V, Fiehn O, Weiss RH. A comprehensive urinary metabolomic approach for identifying kidney cancerr. Anal Biochem 2007;363:185-95.
30. Nishiumi S, Kobayashi T, Ikeda A, et al. A novel serum metabolomics-based diagnostic approach for colorectal cancer. PLoS One 2012;7:e40459.
31. Wibom C, Surowiec I, Moren L, et al. Metabolomic patterns in glioblastoma and changes during radiotherapy: a clinical microdialysis study. Journal of proteome research 2010;9:2909-19.
32. Frontera JA, Claassen J, Schmidt JM. Prediction of Symptomatic Vasospasmafter Subarachnoid Hemorrhage: the Modified Fisher Scale. … 2006.
33. Hunt WE, Hess RM. Surgical risk as related to time of intervention in the repair of intracranial aneurysms. Journal of neurosurgery 1968.
34. Seiler RW, Grolimund P, Aaslid R, Huber P. Cerebral vasospasm evaluated by transcranial ultrasound correlated with clinical grade and CT-visualized subarachnoid hemorrhage. Journal of … 1986.
35. Vergouwen MDI. Vasospasm versus delayed cerebral ischemia as an outcome event in clinical trials and observational studies. Neurocritical care 2011.
36. Jennett B, Bond M. Assessment of outcome after severe brain damage: a practical scale. The Lancet 1975.
37. Fiehn O, Wohlgemuth G, Scholz M, Kind T. Quality control for plant metabolomics: reporting MSI-compliant studies. Plant J 2008;53:691-704.
38. Sansone S-A, Fan T, Goodacre R, et al. The Metabolomics Standards Initiative. Nature Biotechnology 2007;25:846-8.
39. Shaw E, Scott C, Souhami L, Dinapoli R, Kline R. Single dose radiosurgical treatment of recurrent previously irradiated primary brain tumors and brain metastases: final report of RTOG protocol 90-05. International Journal of … 2000.
40. Sjöberg RL, Bergenheim T, Mörén L, Antti H. Blood Metabolomic Predictors of 1-Year Outcome in Subarachnoid Hemorrhage. Neurocritical Care 2015;23:225-32.

41. Sajanti J, Heikkinen E, Majamaa K. Rapid induction of meningeal collagen synthesis in the cerebral cisternal and ventricular compartments after subarachnoid hemorrhage. Acta Neurochirurgica 2001;143:821-6.
42. Dang L, White DW, Gross S, et al. Cancer-associated IDH1 mutations produce 2-hydroxyglutarate. Nature 2009;462:739-44.
43. Choi C, Ganji SK, DeBerardinis RJ, Hatanpaa KJ. 2-hydroxyglutarate detection by magnetic resonance spectroscopy in IDH-mutated patients with gliomas. Nature Medicine 2012;18:624-9.
44. Oldham WM, Clish CB, Yang Y, Loscalzo J. Hypoxia-mediated increases in L-2-hydroxyglutarate coordinate the metabolic response to reductive stress. Cell Metabolism 2015;22:291-303.
45. Intlekofer AM, Dematteo RG, Venneti S, Finley LWS. Hypoxia induces production of L-2-hydroxyglutarate. Cell Metabolism 2015;22:304-11.
46. Worth AJ, Gillespie KP, Mesaros C, et al. Rotenone stereospecifically increases (S)-2-hydroxyglutarate in SH-SY5Y neuronal cells. Chemical Research in Toxicology 2015;28:948-54.
47. Park HS, Wang EH, Rutter CE, Corso CD, Chiang VL, Yu JB. Changing practice patterns of Gamma Knife versus linear accelerator-based stereotactic radiosurgery for brain metastases in the US. J Neurosurg 2016;124:1018-24.
48. Sneed PK, Mendez J, Vemer-van den Hoek JG, et al. Adverse radiation effect after stereotactic radiosurgery for brain metastases: incidence, time course, and risk factors. J Neurosurg 2015;123:373-86.
49. Verma N, Cowperthwaite MC, Burnett MG, Markey MK. Differentiating tumor recurrence from treatment necrosis: a review of neuro-oncologic imaging strategies. Neuro Oncol 2013;15:515-34.
50. Burger PC, Boyko OB. The pathology of central nervous system radiation injury. Radiation injury to the nervous system. NY: Raven; 1991:191-208.
51. Castel JC, Caille JM. Imaging of irradiated brain tumours. Value of magnetic resonance imaging. J Neuroradiol 1989;16:81-132.
52. Kimura T, Sako K, Gotoh T, Tanaka K, Tanaka T. In vivo single-voxel proton MR spectroscopy in brain lesions with ring-like enhancement. NMR in biomedicine 2001;14:339-49.
53. Shah R, Vattoth S, Jacob R, et al. Radiation necrosis in the brain: imaging features and differentiation from tumor recurrence. Radiographics 2012;32:1343-59.
54. Zhao Q, Cao Y, Wang Y, et al. Plasma and tissue free amino acid profiles and their concentration correlation in patients with lung cancer. Asia Pac J Clin Nutr 2014;23:429-36.
55. Liu W, Hancock CN, Fischer JW, Harman M, Phang JM. Proline biosynthesis augments tumor cell growth and aerobic glycolysis: involvement of pyridine nucleotides. Scientific reports 2015;5:17206.
56. Sodi VL, Khaku S, Krutilina R, et al. mTOR/MYC Axis Regulates O-GlcNAc Transferase Expression and O-GlcNAcylation in Breast Cancer. Molecular cancer research : MCR 2015;13:923-33.
57. Wikoff WR, Grapov D, Fahrmann JF, et al. Metabolomic markers of altered nucleotide metabolism in early stage adenocarcinoma. Cancer prevention research (Philadelphia, Pa) 2015;8:410-8.

58. Corbett RJ, Nunnally RL, Giovanella BC, Antich PP. Characterization of the 31P nuclear magnetic resonance spectrum from human melanoma tumors implanted in nude mice. Cancer Res 1987;47:5065-9.

Figure References and Legends

Figure 1: Principal component analysis of CSF samples collected at admission vs. during hospitalization.

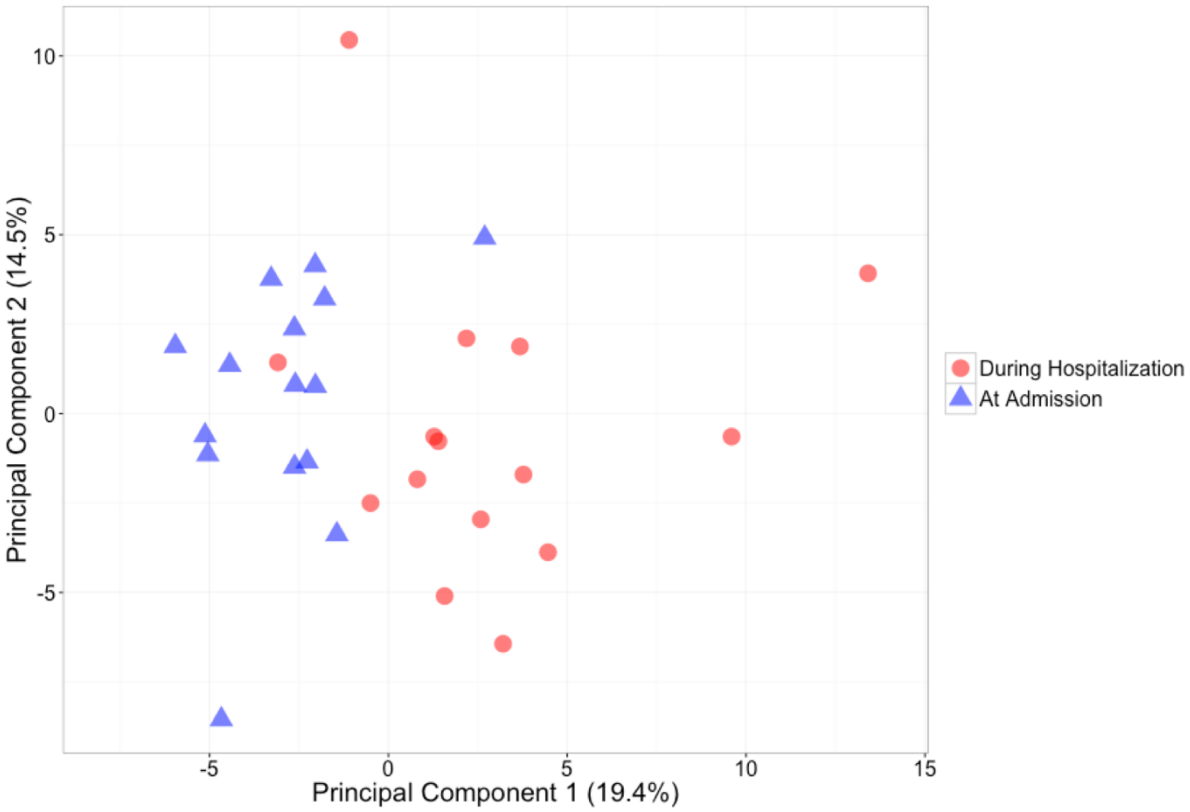

Figure 2: Metabolites significantly change from time at admission to time during hospitalization

A. 16 metabolites significantly change between time at admission to time during hospitalization.

B. Of the 16 metabolites measured at hospitalization, changes were magnified with higher modified Fisher grade (4 vs. 3). Nine of these metabolites had $p<0.05$.

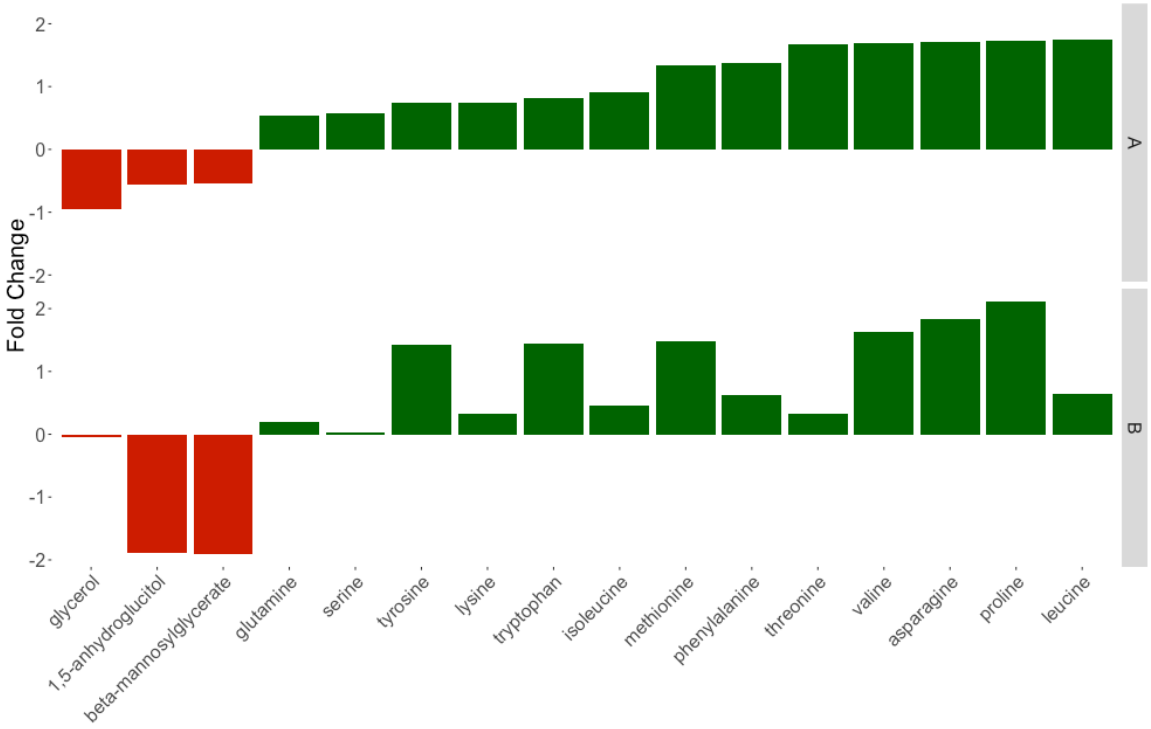

Figure 3: Relative 2-hydroxygluarate levels and receiver operating characteristic curve of 2-hydroxyglutarate at predicting patients with low disability (GOS=5) at 1-Year Post-aSAH. 3A.

- For patients with GOS=5, 2-hydroxyglutarate trended to decrease whereas for patients with GOS≤4, 2-hydroxyglutarate trended to increase. 3B. Area-under-curve value of 0.85 for the receiver operating characteristic curve of 2-hydroxyglutarate.

A.

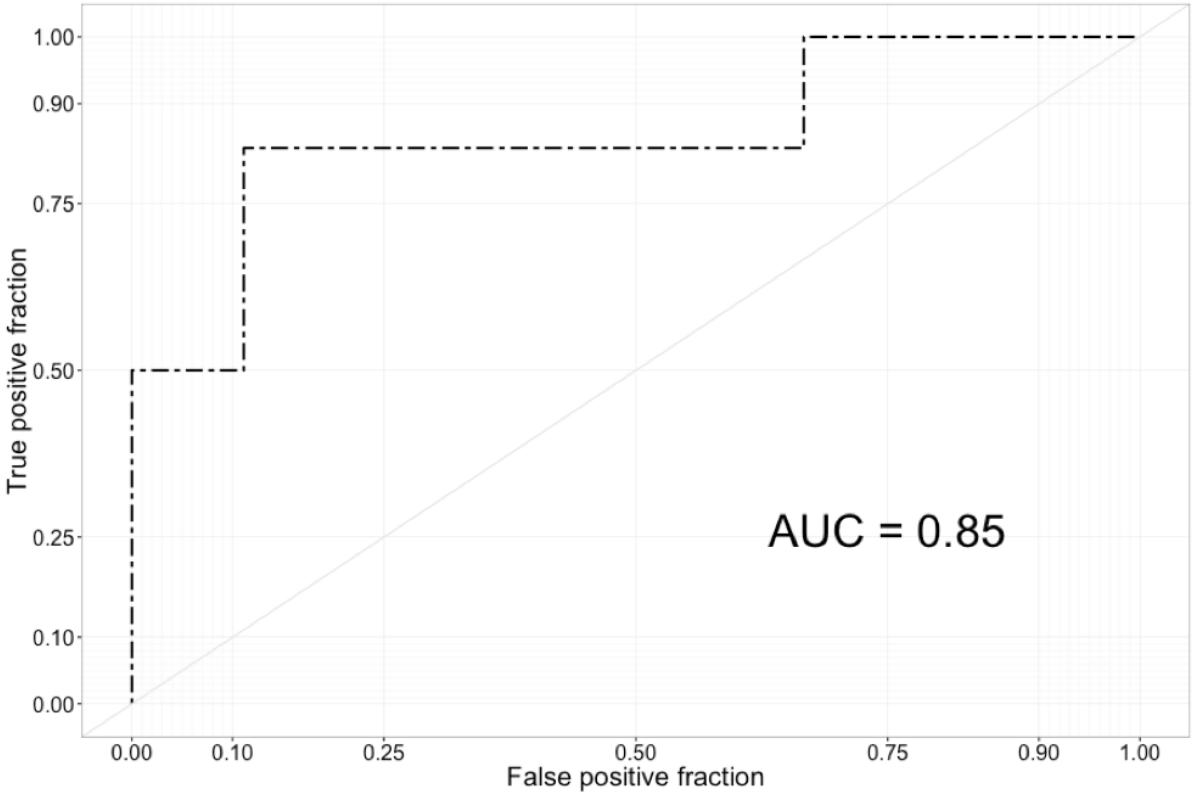

B.

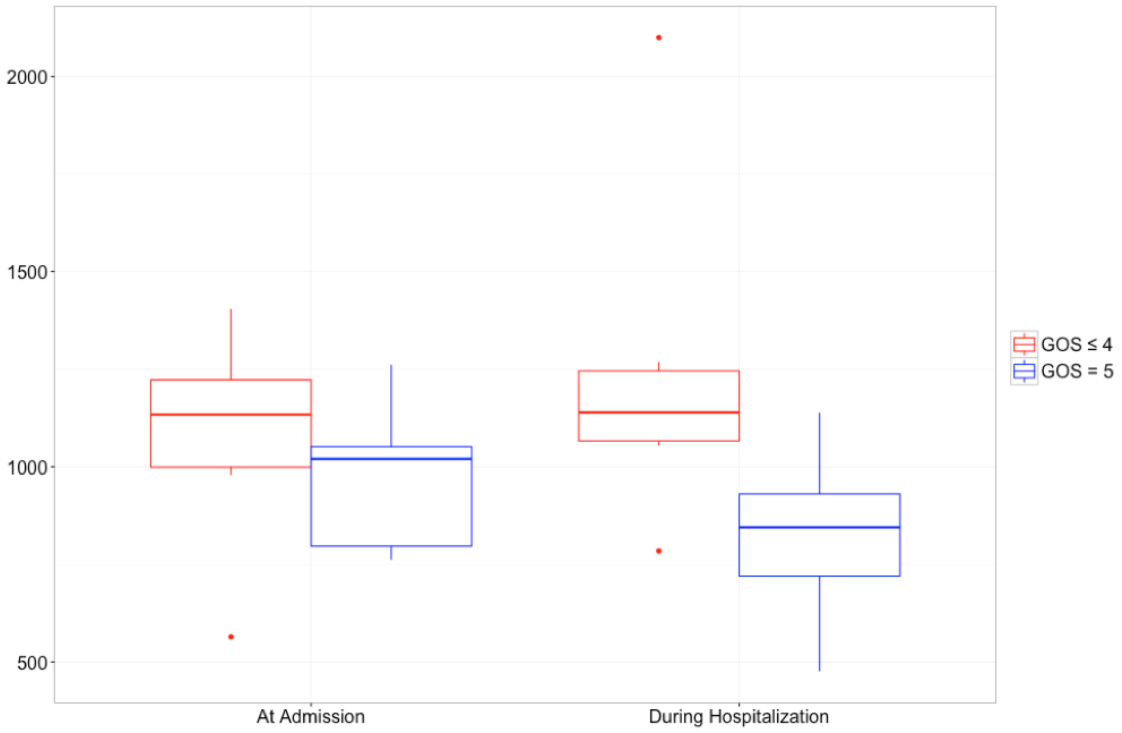
2000
1500
1000
500
At Admission
During Hospitalization
GOS ≤ 4
GOS = 5

Figure 4: Patients with low disability (GOS=5) trend to have lower levels of alpha-ketoglutarate and 2-hydroxyglutarate whereas patients with higher disability (GOS≤4) trend to have higher levels of alpha-ketoglutarate and 2-hydroxyglutarate during aSAH hospital course

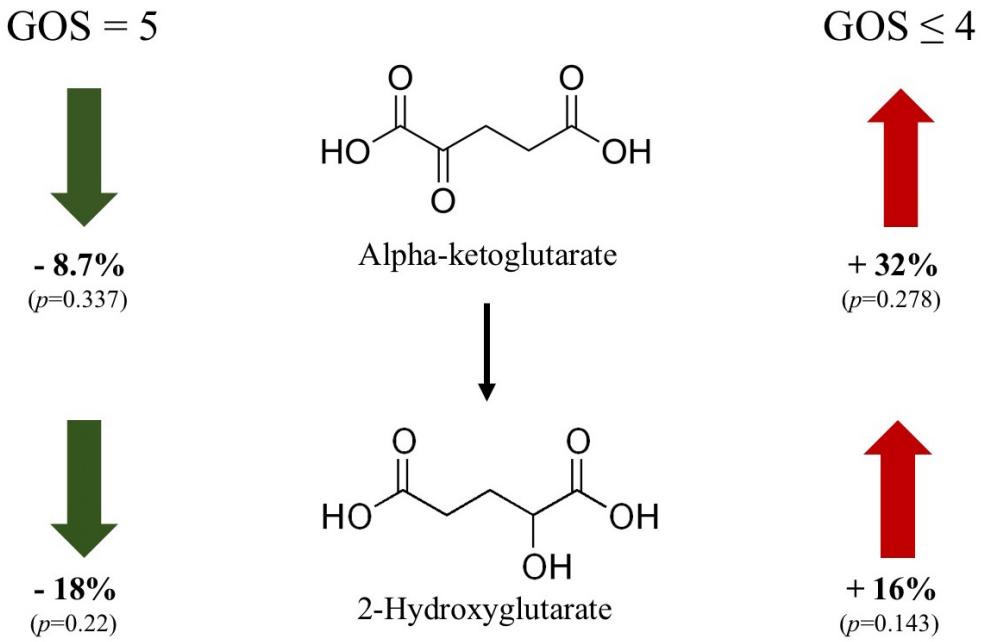

Figure 5: Histology of Radiation Necrosis and Tumor

- The identity of each flash frozen sample was confirmed histologically. Radiation necrosis at 200x (A) & 400x (B) magnification, H&E. Radiation necrosis was defined as inflammatory demyelination and reactive gliosis in the absence of tumor cells. Recurrent non-small cell lung cancer at 200x (C) & 400x (D) magnification, H&E. Metastatic tumors from various primary tumors were also identified histologically.

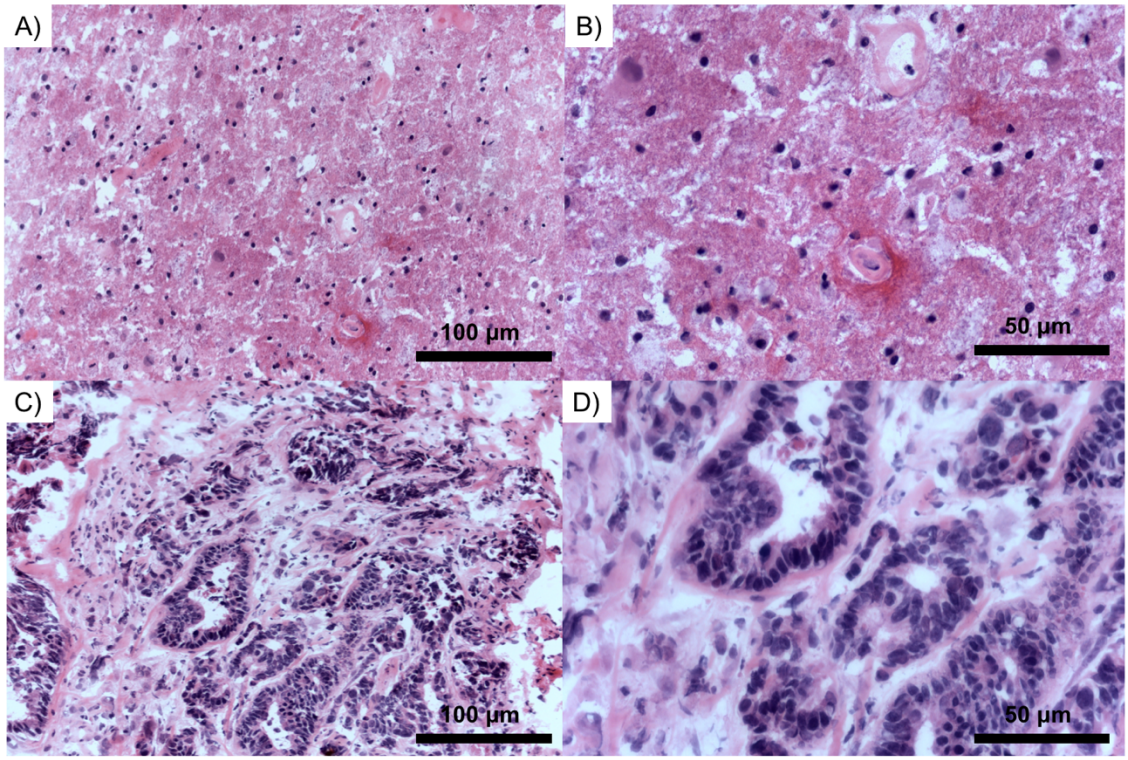

Figure 6: Principal Component Analysis Plots and Random Forest Analysis Shows High Discrimination Accuracy Between Radiation Necrosis and Tumor

A) Principal component analysis score plot showing differential variance between tumor and radiation necrosis as well as primary tumor types.

B) Random forest analysis identifies a ranked list of metabolites for classification of tumor versus radiation necrosis.

A.

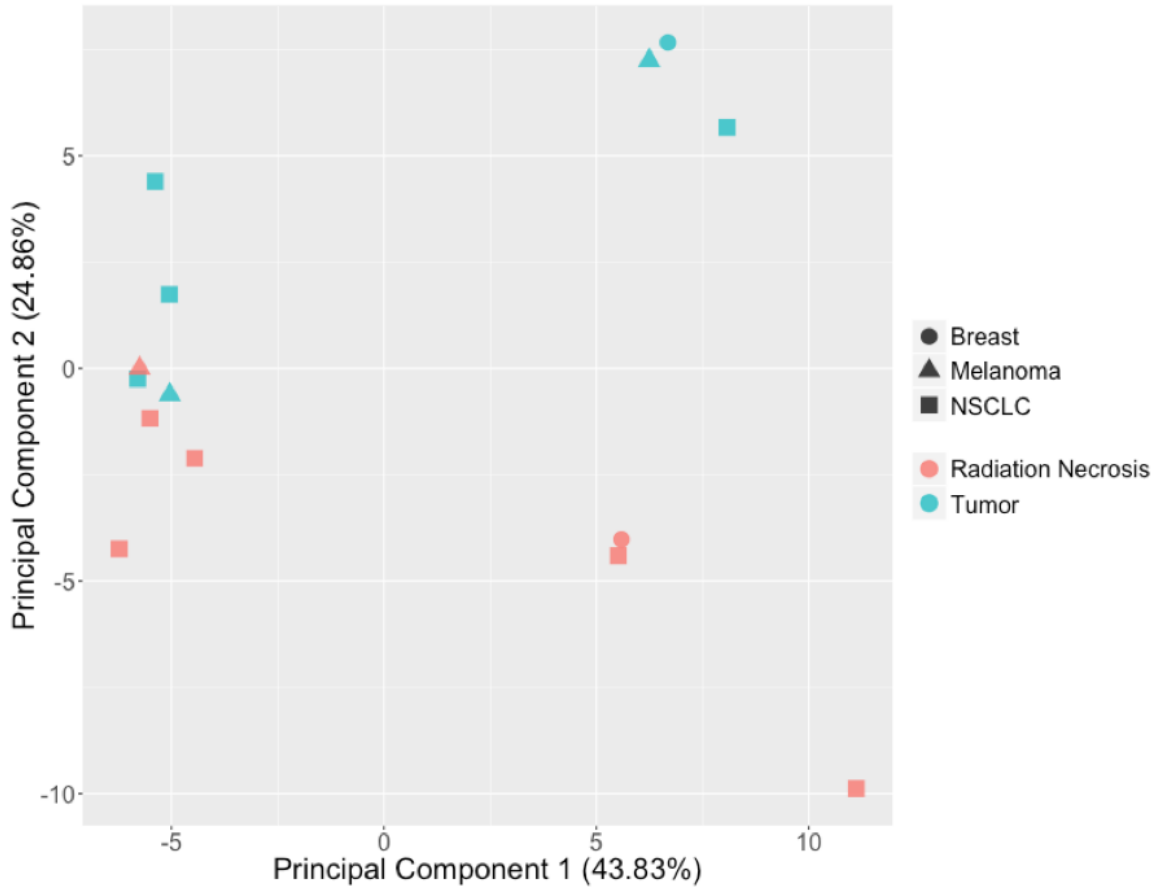

B.

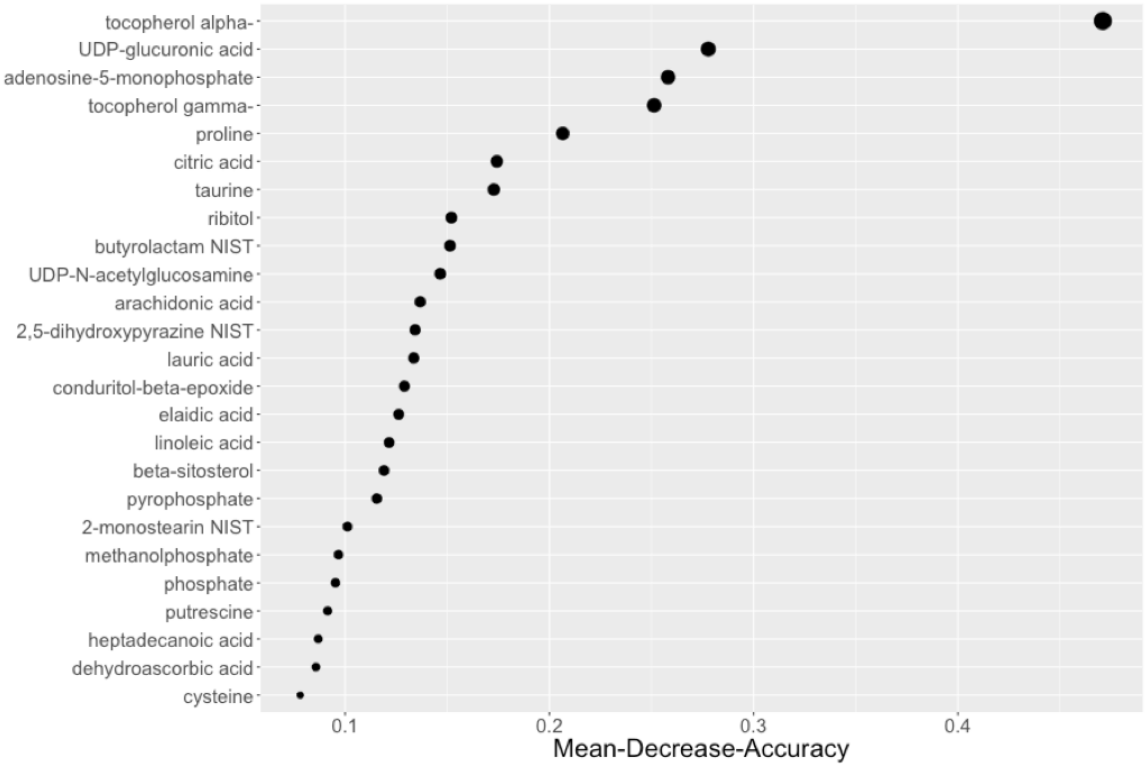
tocopherol alpha-
UDP-glucuronic acid
adenosine-5-monophosphate
tocopherol gamma-
proline
citric acid
taurine
ribitol
butyrolactam NIST
UDP-N-acetylglucosamine
arachidonic acid
2,5-dihydroxypyrazine NIST
lauric acid
conduritol-beta-epoxide
elaidic acid
linoleic acid
beta-sitosterol
pyrophosphate
2-monostearin NIST
methanolphosphate
phosphate
putrescine
heptadecanoic acid
dehydroascorbic acid
cysteine
0.1
0.2
0.3
0.4
Mean-Decrease-Accuracy

Figure 7: Heatmap of Significant Metabolites Reveals Metabolic Signatures of Radiation Necrosis and Tumor

- An unsupervised hierarchical clustering analysis shows 3 distinct clusters of metabolites that discriminate radiation necrosis and tumor. Metabolites that represent increased metabolism were elevated in tumor. Metabolites that represent fatty acid products and antioxidants/cofactors were elevated in radiation necrosis.

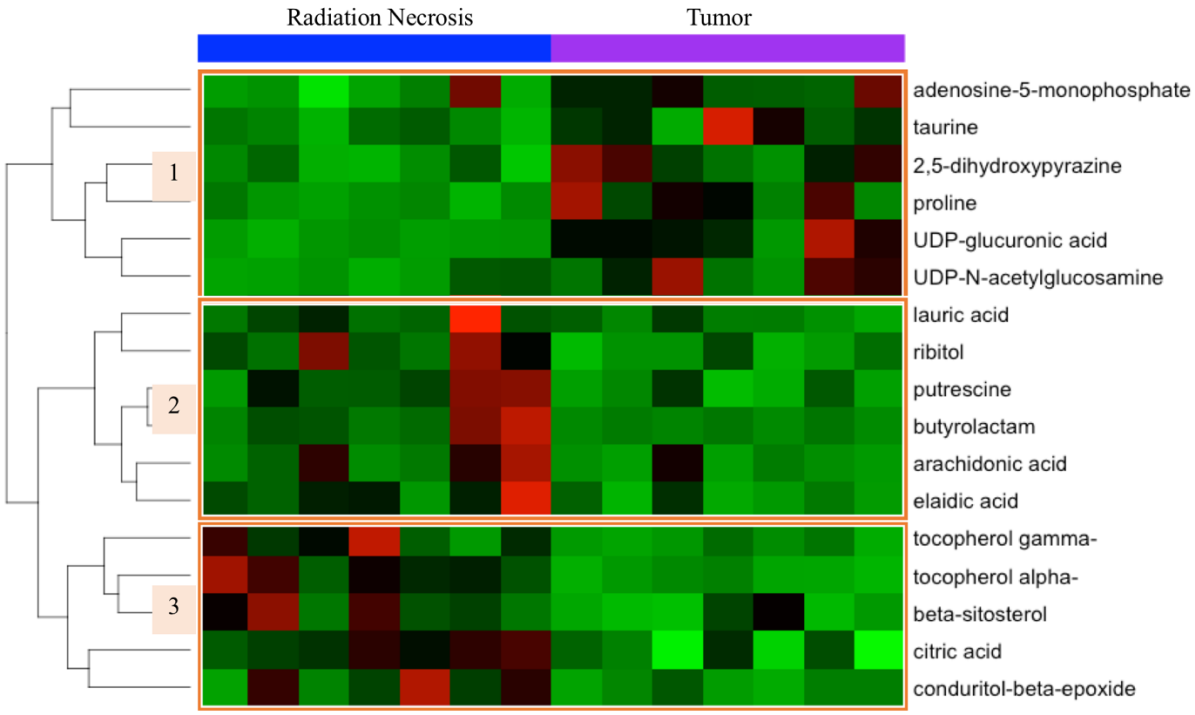

Figure 8: Boxplots and Receiver Operating Characteristic Curves for Selected Metabolites Discriminating Between Tumor and Radiation Necrosis

- Selected metabolites provide a high degree of discrimination between tumor and radiation necrosis according to the area-under-curve values of the receiver operating characteristic curves.

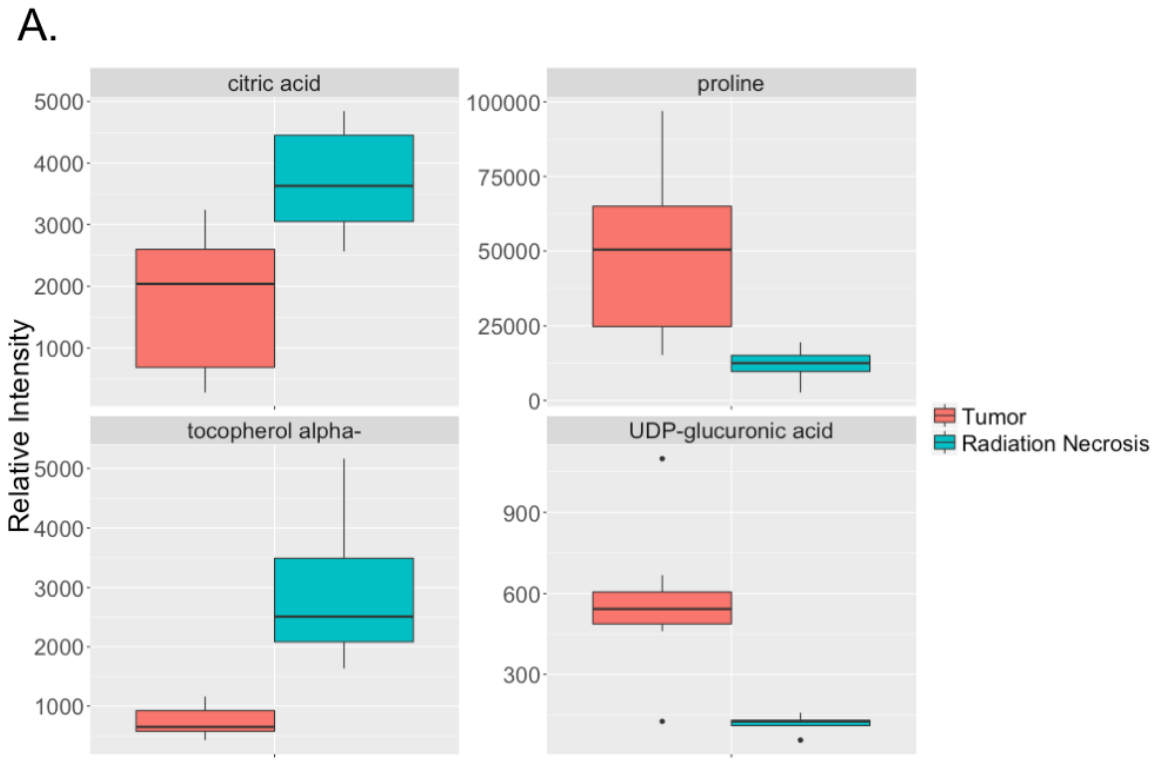

B.

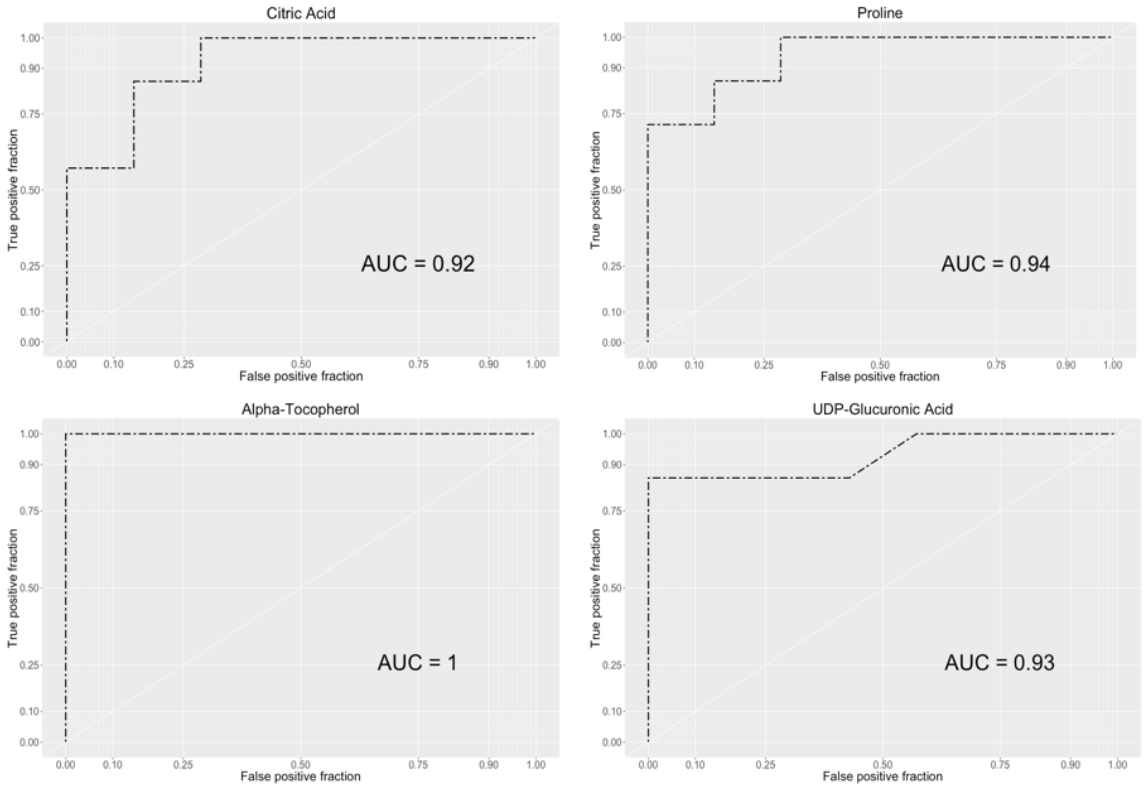
Citric Acid
AUC = 0.92
Proline
AUC = 0.94
Alpha-Tocopherol
AUC = 1
UDP-Glucuronic Acid
AUC = 0.93
True positive fraction
False positive fraction
0.00
0.10
0.25
0.50
0.75
0.90
1.00

Tables.

Table 1: Patient demographics and characteristics

H&H = Hunt and Hess Scale; GOS = Glasgow Outcome Scale; A-Comm = anterior communicating artery; P-Comm = posterior communication artery; VA = vertebral artery; ICA = internal carotid artery; MCA = middle cerebral artery

Patient ID	Age	Gender	Smoking	Hypertension	aSAH treatment	Aneurysm Site	Cerebral Vasospasm	Modified Fisher	H&H	GOS
1	54	F	+	+	Coiling	R P-Comm	+	4	4	5
2	24	M	+	−	Coiling	A-Comm	+	3	4	4
3	63	M	−	−	L VA Closure	L VA	+	3	4	5
4	56	F	−	−	Coiling	R P-Comm	+	4	4	5
5	48	M	+	+	Coiling	A-Comm	+	3	2	5
6	57	F	+	−	Coiling	A-Comm	+	4	3	1
7	49	F	−	+	Clipping	A-Comm	+	4	3	5
8	40	F	+	−	Clipping	A-Comm	+	3	3	5
9	68	M	+	+	Clipping	A-Comm	+	3	3	5
10	28	F	+	−	Coiling	A-Comm	−	3	4	4
11	74	F	+	+	Clipping	L MCA	−	4	5	3
12	88	F	−	+	Coiling	L Superior Cerebellar	−	4	4	1
13	51	F	+	+	Coiling	A-Comm, L Supraclinoid ICA	−	3	2	5
14	68	F	+	−	Clipping	R MCA	−	4	5	5
15	68	F	−	+	Coiling	A-Comm	−	3	4	4

Table 2: CSF collection listed by post-bleed day

Patient ID	Post-Bleed Collection Day (At Admission)	Post-Bleed Collection Day (During Hospitalization)
1	1	4
2	0	5
3	2	3
4	1	6
5	2	4
6	1	7
7	2	5
8	0	9
9	1	4
10	1	6
11	1	5
12	0	3
13	2	6
14	1	10
15	1	6

Table 3: Metabolites significantly change from time at admission to time during hospitalization

*Significant after Bonferroni correction; KEGG ID = Kyoto Encyclopedia of Genes and Genomes identifier; NS = Not Significant

Metabolite	KEGG	Nominal *p*-Value	Bonferroni Correction	Fold Change	Nominal *p*-Value (Fisher)	Fold Change (Fisher)
phenylalanine	C00079	2.47E-05	*	1.37	5.91E-03	0.63
leucine	C00123	3.95E-05	*	1.75	2.89E-02	0.65
threonine	C00188	4.39E-05	*	1.67	NS	0.32
valine	C00183	7.10E-05	*	1.69	2.89E-02	1.63
tryptophan	C00078	7.22E-05	*	0.82	2.05E-02	1.45
serine	C00065	8.51E-05	*	0.58	NS	0.02
glycerol	N/A	8.92E-05	*	-0.96	NS	-0.04
1,5-anhydroglucitol	C07326	1.38E-04	*	-0.55	2.05E-02	-1.89
methionine	C00073	1.45E-04	*	1.34	4.01E-02	1.48
beta-mannosylglycerate	N/A	2.29E-04	*	-0.54	2.05E-02	-1.91
asparagine	C00152	4.31E-04	*	1.70	1.40E-02	1.83
tyrosine	C00082	5.15E-04	*	0.74	3.73E-03	1.43
lysine	C00047	1.08E-03	NS	0.75	NS	0.33
glutamine	C00064	1.10E-03	NS	0.54	NS	0.20
isoleucine	C00407	4.53E-03	NS	0.91	NS	0.46
proline	C00148	1.04E-02	NS	1.73	NS	2.12

Table 4: Metabolites significantly correlate with 1-year outcome post-aSAH

*Significant after Bonferroni correction; KEGG ID = Kyoto Encyclopedia of Genes and Genomes identifier; NS = Not Significant

Metabolite	KEGG ID	Nominal *p*-Value	Bonferroni Correction	Pearson's Correlation Coefficient
2-Hydroxyglutarate	C02630	4.54E-04	*	-0.79
Tryptophan	C00078	7.16E-04	NS	-0.774
Glycine	C00037	9.51E-04	NS	-0.762
Proline	C00148	1.24E-03	NS	-0.751
Isoleucine	C00407	1.61E-03	NS	-0.74
Alanine	C00041	2.2E-03	NS	-0.726

Table 5: Patient Demographics

- Radiation necrosis and tumor specimens were obtained from 10 patients who underwent Gamma Knife radiosurgery

NSCLC: non-small cell lung cancer, WT: wild type

Patient ID	Sex	Age at Biopsy	Primary Tumor Type	Primary Tumor Subtype & Mutation Studies	GKRS until Resection (Days)	Medications at Time of Resection
1	F	47	NSCLC	Adenocarcinoma (ALK WT, AKT WT, BRAF WT, EGFR WT, ERB2 WT, KRAS WT, MEK1 WT, PIK3CA WT)	295	Kefzol (1g), Decadron (10mg), Mannitol (25g), Alprazolam (.5mg PRN), Chlorpheniramine-hydrocodone (8mg every 12 hours), Colace
2	F	66	NSCLC	Adenocarcinoma (ALK WT, EGFR WT, KRAS Q16H)	181	Ceftriaxone (1g), Vancomycin (1g), Mannitol (25g), Decadron (10mg), Vitamin C (250mg BID), Citalopram (10mg daily), Keppra (500mg BID), Zinc Sulfate (220mg daily)
3	F	71	NSCLC	Adenocarcinoma (ALK WT, AKT1 WT, BRAF WT, EGFR WT, ERBB2 WT, KRAS WT, MEK1 WT, PIK3CA WT, ROS1 WT)	496	Acetaminophen (650mg every 6 hours), Acidophilus (1 day), Amlodipine (5mg), Bromday drops, Lactaid, Levothyroxine (150mcg daily), Lorazepam (.25mg PRN), Omeprazole (50mg daily), Sertraline (50mg daily), Timolol drops, Kefzol (1g), Keppra (500mg), Decadron (10mg), Mannitol (50g), Lasix (20mg)
4	F	50	NSCLC	Adenocarcinoma (EGFR WT, BRAF WT, AKT WT, MEK1 WT)	99	Kefzol (1g), Mannitol (25g), Lasix (40mg), Decadron (10mg)
5	F	40	Melanoma	BRAF V600E	98	Kefzol (1g), Decadron (10mg), Mannitol (25g), Vemurafenib (750mg BID), Multivitamin, Omeprazol (20mg daily), Keppra (150mg BID)
6	M	57	Melanoma	BRAF WT	76	Kefzol (1g), Decadron (10mg), Mannitol (25g), Vitamin D (1000U daily)
7	F	66	Breast	ER+, PR+, HER2+	-8*	Vitamin C (1000mg daily), Colace (100mg daily), Metoprolol (50mg daily), Ondansetron (8mg PRN), Valsartan-hydrochlorothiazide (320mg daily), Vitamin D (50,000 units weekly). Kefzol (1g), Mannitol (25g), Lasix (20mg), Decadron (10mg)
8	F	50	Breast	ER-, PR-, HER2 Equivocal	1604	Decadron (10mg), Kefzol (1g), Keppra (500mg), Trastuzumab (every three weeks), Tykerb (250mg daily), Ativan (1mg PRN), Glycolax, Zolpidem (PRN), Insulin aspart (dates unclear)
9	M	35	Melanoma	BRAF V600E	-1*	Kefzol (1g), Decadron (10mg), Mannitol (25g), Pantoprazole (40mg daily)
10	F	57	NSCLC	Adenocarcinoma (KRAS G12V, EGFR WT)	517	Kefzol (1g), Mannitol (.5g/kg), Decadron (10mg), Lasix (20mg)

Table 6: Pathology Characteristics

- Multiple primary tumor types were analyzed in an attempt to generalize our findings. Seven samples of tumor were compared to 7 samples of demyelinating radiation necrosis.

  *Two samples of tumor included for metabolomic analysis were not irradiated prior to resection; these patients underwent GKRS after resection

  NSCLC: non-small cell lung cancer, WT: wild type

Specimen ID	Patient ID	Primary Tumor Type	Pathology	Biopsy Location
1	1	NSCLC	Recurrent Tumor	Frontal
2	1	NSCLC	Radiation Necrosis	Frontal
3	2	NSCLC	Recurrent Tumor	Frontal
4	2	NSCLC	Radiation Necrosis	Frontal
5	3	NSCLC	Recurrent Tumor	Frontoparietal
6	3	NSCLC	Radiation Necrosis	Frontoparietal
7	3	NSCLC	Recurrent Tumor	Frontoparietal
8	4	NSCLC	Radiation Necrosis	Parietal
9	5	Melanoma	Recurrent Tumor	Frontal
10	6	Melanoma	Radiation Necrosis	Frontal
11	7	Breast	Metastatic Tumor	Cerebellar
12	8	Breast	Radiation Necrosis	Frontoparietal
13	9	Melanoma	Metastatic Tumor	Right Frontal
14	10	NSCLC	Radiation Necrosis	Temporal

Table 7: Significant Metabolites Changes Between Radiation Necrosis and Tumor

- Identified metabolites from RF analysis were analyzed using Mann-Whitney *U* test. Positive mean fold indicates elevated levels in Radiation Necrosis; negative fold change indicated elevated levels in tumor. KEGG database identifiers are also displayed. In this analysis, 17 metabolites with known structures had *p*-value < 0.05 and fold change > 0.5.

  *KEGG ID: Kyoto Encyclopedia of Genes and Genomes identifier

  NSCLC: non-small cell lung cancer

Metabolites	KEGG ID	Fold Change	Nominal *P*-Value
Alpha-Tocopherol	C02477	2.91	5.83E-04
Proline	C00148	-3.04	4.08E-03
Citric acid	C00158	1.15	6.99E-03
Gamma-Tocopherol	C02483	2.75	6.99E-03
UDP-Glucuronic Acid	C00167	-3.81	8.66E-03
Butyrolactam	C11118	5.89	1.11E-02
2,5-Dihydroxypyrazine	NA	-2.05	1.75E-02
Arachidonic Acid	C00219	1.63	1.75E-02
Elaidic Acid	C00712	0.86	1.75E-02
Taurine	C00245	-2.21	1.75E-02
UDP-N-Acetylglucosamine	C00043	-2.11	1.75E-02
Ribitol	C00474	1.94	2.13E-02
Adenosine-5-Monophosphate	C00020	-0.87	2.62E-02
Beta-Sitosterol	C01753	1.18	2.62E-02
Conduritol-Beta-Epoxide	NA	2.13	3.79E-02
Lauric Acid	C02679	0.91	3.79E-02
Putrescine	C00134	1.47	3.79E-02